Wind power system connected to the grid from Squirrel Cage Induction Generator (SCIG)

Ângelo Marcílio M. dos Santos
PPGEEC/UFC, Campus Sobral
Federal University of Ceará
Sobral-CE, Brazil
angelomarcilio@alu.ufc.br

Ildenor Davi S. Júnior
PPGEEC/UFC, Campus Sobral
Federal University of Ceará
Sobral-CE, Brazil
juniordavid1208@gmail.com

Lucas Taylan P. Medeiros
PPGEEC/UFC, Campus Sobral
Federal University of Ceará
Sobral-CE, Brazil
lucastaylanp@gmail.com

Leonardo P. S. Silva
Electrical Engineering, Campus Sobral
Federal University of Ceará
Sobral-CE, Brazil
leonardo85pires@gmail.com

Vanessa Siqueira de C. Teixeira
PPGEEC/UFC, Campus Sobral
Federal University of Ceará
Sobral-CE, Brazil
vanessasct@gmail.com

Adson Bezerra Moreira
PPGEEC/UFC, Campus Sobral
Federal University of Ceará
Sobral-CE, Brazil
adsonbmoreira@gmail.com

***Abstract*—This research aims to present a wind power system connected to electric grid using the three-phase induction generator with a squirrel cage rotor (SCIG). The SCIG stator terminals are connected to electric grid before the inductive filter using an AC/DC/AC power converter topology, called back-to-back, while the rotor terminals are short circuited, so that the SCIG's active and reactive power control techniques are presented. The control of grid side converter (GSC) is presented, responsible for the power control and also for keeping the DC bus voltage constant. The control of induction generator side converter (IGSC) is presented also, in which vector control is used in rotor variables, so that the SCIG is controlled through the torque references and magnetizing current. The studied system was mathematically modeled and simulated using Matlab/Simulink software.**

***Keywords* – Controllers design. Electric power generation. Electronic back-to-back converter. SCIG. Wind energy.**

I. Introduction

With the progressive decline of fossil fuels reserves and ever-increasing demand of energy, the production of electric energy from renewable resources, such as solar, wind and tidal streams oceans, has now been accepted as a potentially promising solution to the energy problem [8]. Of these, wind power is one of an effective mitigation measures, the development of wind power generation has increasingly attracted attention in various countries [9].

There are several types of electric generators used in wind power system. This way, the choice of wich type of electric generator depends on the application of a distributed machine, wind farms, electric transmission, machine power and cost [11].

In this paper a squirrel cage induction generator (SCIG) is used because are extensively employed for power generation from wind energy due to simple and rugged rotor construction, low cost, almost nil maintenance and generator operation without the need of DC supply [7].

Besides that, wind turbines based on (SCIG) with back-to-back voltage source converter are becoming increasingly popular. Compared with the wind turbines using fixed-speed induction generators, the SCIG-based wind turbines offers not only the advantages of variable speed operation and four-quadrant active and reactive power capabilities, but also separation between grid and generator by conversion of AC-DC-AC [10].

The back-to-back converter is composed of two voltage source converters connected together via a DC bus capacitor. One converter stays between the SCIG and the DC bus capacitor called induction generator side converter (IGSC), which has the function to produce the machine flux for SCIG and to optimum the energy capture from the wind. The second converter stays between the DC bus capacitor and the grid called grid side converter (GSC), which has the function to regulate the DC bus voltage [5].

In this paper, the employed methodology obtains results based on mathematical modeling of the system, shown in Fig. 1. The studies will be conducted through computer simulation with mathematical models of studied system for validation of control strategies, and the SCIG connected to power grid. For the simulations we will use computational tool $SimPowerSystems^{©}$ of $Matlab/Simulink^{©}$.

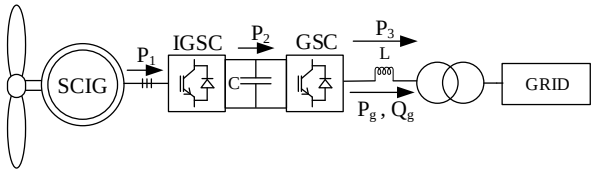

Fig. 1. Wind system studied.

The main contribution of this paper is to present a methodology proposal for the development of active and reactive power

control of a wind power generation system connected to the grid from a SCIG.

The paper is structured as follows: Section II describes the modeling of the GSC control system. The section III describes the modeling of the IGSC control system. The section IV describes the analysis and results. Finally, in the section V exposes the conclusions.

II. Grid Side Converter - GSC

The grid side converter, a three-phase DC-to-AC electronic converter, controls the DC bus voltage constant and the current injected into the grid [2].

GSC control is performed by the block diagram of Fig. 2, in which the current loop is shown in Fig. 2 (a) and the voltage loop in Fig. 2 (b) [3].

The PLL (phase locked loop) is responsible for maintaining the synchronism between the voltages of the grid and those produced by the inverter, generating an angle θ in phase with the grid voltage, where V_A, V_B and V_C are grid line voltages.

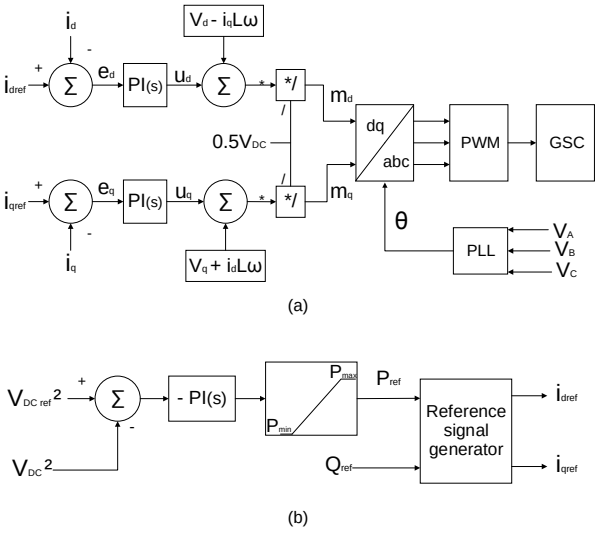

Fig. 2. Grid side converter control scheme (current loop (a) and voltage loop (b)).

The current control loop I_d (direct axis current) shows I_{dref} (direct axis reference current) as a reference from the DC bus voltage control. In the current control loop I_q (quadrature axis current) , assumed I_{qref} (quadrature axis reference current) $= 0$, making the converter operate with unit power factor. The signal reference generator produces current references, (I_{dref} and I_{qref}), from (1) and (2), where V_{sd} and V_{sq} are the phase voltages of the grid in dq coordinates.

$$P_{sref} = \frac{3}{2}\left[V_{sd}\, i_{dref} \;+\; V_{sq}\, i_{qref}\right] \tag{1}$$

$$Q_{sref} = \frac{3}{2}\left[-V_{sd}\, i_{qref} \;+\; V_{sq}\, i_{dref}\right] \tag{2}$$

Since $V_q = 0$, (1) and (2) can be simplified as (3) and (4).

$$i_{dref} = \frac{2}{3V_{sd}}\, P_{sref} \tag{3}$$

$$i_{qref} = -\frac{2}{3V_{sd}}\, Q_{sref} \tag{4}$$

A. GSC DC bus voltage and current control

The design of the controllers is based on the frequency response, so it must have a gain margin (GM) greater than 6 dB and a phase margin (PM) between 30º and 60º [1], [4].

The block representation of the GSC direct and quadrature axis current controllers is shown in Fig. 3, in which the block $PI(s)$ is a PI controller, $G_p(s)$ characterizes the dynamics of the GSC PWM and $G_c(s)$ is the GSC plant with L filter. $G_i(s)$ is the product of blocks $G_p(s)$ and $G_c(s)$ cascading.

The transfer functions $G_p(s)$ e $G_c(s)$ are given, respectively, by (5) and (6), in which T_s is the sampling time, L is the inductance of the filter that connects to the grid to the converter, and R is the electrical resistance present in the inductor [1].

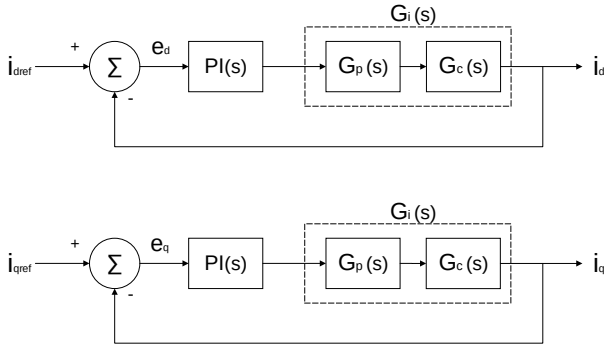

Fig. 3. Simplified block diagram of GSC current controller with L filter at dq coordinates.

$$G_p(s) = \frac{1 \;-\; s(\frac{T_s}{4})}{1 \;+\; s(\frac{T_s}{4})} \tag{5}$$

$$G_c(s) = \frac{1}{Ls \;+\; R} \tag{6}$$

The transfer function of the PI controller is given in (7).

$$PI(s) = \; k_p \; (\; 1 \; + \; \frac{1}{T_i \; s} \;) \tag{7}$$

For $s = j\omega$, it has (8) and (9).

$$PI(j\omega) = \; k_p \; (\; 1 \; + \; \frac{1}{T_i \; j\omega} \;) \tag{8}$$

$$\angle PI(j\omega) = \; - \; arctan \; \frac{1}{T_i \; \omega} \tag{9}$$

The desired phase margin, PM_d, is calculated from (10), where ω_c is the gain crossing frequency.

$$PM_d = \pi \; + \; \angle G_i(j\omega_c) \; + \; \angle PI(j\omega_c) \tag{10}$$

When applying (9) in (10) and when isolating T_i, it is determined (11), the first condition of the controller project.

$$T_i = \frac{1}{\omega_c \cdot tan\,(\,\pi \,+\, \angle G_i(j\omega_c) \,-\, PM_d\,)} \tag{11}$$

According to [1], the magnitude of the open-loop transfer function of a controlled system is the unit at the crossing frequency, obtaining (12). Substituting (8) into (12) and isolating k_p, the second controller project condition is given by (13).

$$|PI(j\omega_c| \cdot |G_i(j\omega_c| \,=\, 1 \tag{12}$$

$$k_p \,=\, \frac{1}{|G_i(j\omega_c| \cdot \left|1 \,-\, \frac{j}{\omega_c\, T_i}\right|} \tag{13}$$

From (11) and (13), to $\omega_c = 1000$ rad/s and $PM = 60^{\text{o}}$, $k_p = 4.9747$ and $T_i = 0.0014$ were obtained for the current controller of the GSC.

The dynamics of the DC bus voltage controller of the GSC is represented by Fig. 4, where block $PI(s)$ is a PI controller, $G_{if}(s)$ is the closed loop of GSC electric current control and $G_{vcc}(s)$ characterizes the DC voltage dynamics of the DC bus.

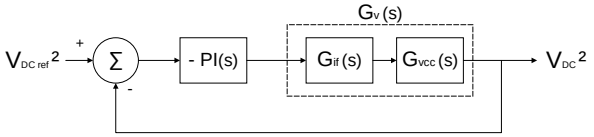

Fig. 4. Simplified block diagram of DC bus voltage controller.

The transfer function $G_{vcc}(s)$ is given by (14), where C is the equivalent capacitance of the AC-DC converter and τ is described in (15), with P_{exto} being the active power.

$$G_{vcc}(s) = \,-\,(\frac{2}{C})\,\frac{\tau s \,+\, 1}{s} \tag{14}$$

$$\tau = \frac{2L\; P_{exto}}{3V_{sd}^2} \tag{15}$$

Applying the project methodology of the PI controllers and adopting $\omega_c = 202\ rad/s$ and $PM = 60^{\text{o}}$, $k_p = 0.3143$ and $T_i = 0.0143$ were obtained for the GSC voltage controller.

III. Induction Generator Side Converter - IGSC

This section describes the main control loop of induction generator side converter. The outputs of the systems control loop are voltage reference used to command the PWM (pulse wide modulation).

The inner of the systems loop controls current by using the model equations of SCIG represented in terms of d-axis, q-axis rotor flux reference frame. The currents are controlled using a standard indirect vector control [6].

A. Squirrel Cage Induction Generator (SCIG)

The equations that govern the dynamics of the AC generator, three-phase and symmetric are represented as (16) to (23), where the dispersion factors of the stator (σ_e) and the rotor (σ_r) are described in (24) and (25) [3].

$$\frac{d\lambda_{ed}}{dt} = V_{ed} \,-\, R_e\; i_{ed} \tag{16}$$

$$\frac{d\lambda_{eq}}{dt} = V_{eq} \,-\, R_e\; i_{eq} \tag{17}$$

$$\frac{d\lambda_{rd}}{dt} = V_{rd} \,-\, R_r\; i_{rd} \tag{18}$$

$$\frac{d\lambda_{rq}}{dt} = V_{rq} \,-\, R_r\; i_{rq} \tag{19}$$

$$\lambda_{ed} = L_m\,[(1+\sigma_e)\; i_{ed} \,+\, e^{j\theta_r}\; i_{rd}] \tag{20}$$

$$\lambda_{eq} = L_m\,[(1+\sigma_e)\; i_{eq} \,+\, e^{j\theta_r}\; i_{rq}] \tag{21}$$

$$\lambda_{rd} = L_m\,[(1+\sigma_r)\; i_{rd} \,+\, e^{-j\theta_r}\; i_{ed}] \tag{22}$$

$$\lambda_{rq} = L_m\,[(1+\sigma_r) i_{rq} \,+\, e^{-j\theta_r}\; i_{eq}] \tag{23}$$

$$\sigma_e = \frac{L_{le}}{L_m} \,-\, 1 \tag{24}$$

$$\sigma_r = \frac{L_{lr}}{L_m} \,-\, 1 \tag{25}$$

V_{ed} and V_{eq} are the stator voltages, V_{rd} and V_{rq} are the voltages in the rotor, i_{ed} and i_{eq} are the stator currents, i_{rd} and i_{rq} are the currents in the rotor, λ_{ed} and λ_{eq} are the stator concatenated fluxes, λ_{rd} and λ_{rq} are the fluxes concatenated in the rotor, in dq coordinates respectively, R_e and R_r are the stator and rotor resistances, L_m is the magnetization inductance, and θ_r is the rotation angle of the rotor.

In SCIG the rotor terminals are shorted and the rotor current is not measured. Then, $V_{rdq} = 0$ and i_{rdq} are not measured. Thus, the rotor currents in dq coordinates are given by (26) and (27), in which $\hat{i}_{mr}$ is the magnitude of the magnetizing current and ρ is the angle of the rotating axis of stator voltages and currents [3].

$$i_{rd} = \frac{\hat{i}_{mr} \,-\, i_{ed}}{1+\sigma_r}\; e^{-j\theta_r} \tag{26}$$

$$i_{rq} = \frac{-\,i_{eq}}{1+\sigma_r}\; e^{-j\theta_r} \tag{27}$$

The electric torque and the rotor time constant (τ_r) are defined in (28) and (29).

$$T_e = \frac{3}{2}\;\frac{L_m}{1 \,+\, \sigma_r}\;\hat{i}_{mr}\; i_{eq} \tag{28}$$

$$\tau_r = \frac{L_m\ (1\ +\ \sigma_r)}{R_r} \tag{29}$$

The rotating magnetic field velocity and rotor speed are determined in (30) and (31).

$$\omega_m = \frac{d\rho}{dt} \tag{30}$$

$$\omega_r = \frac{d\theta_r}{dt} \tag{31}$$

B. Flux observer

In SCIG the flux observer is required to obtain the magnetizing current, the rotating field angle and the speed of the rotating field.

The flux observer is performed by the block diagram of Fig. 5, and is based on (32) and (33), where $\hat{i}_{mr}$ is set to a constant value and $\hat{i}_{mr}$ = i_{ed}, which is required for a linear torque control by i_{eq} [3].

$$\tau_r\ \frac{d}{dt}\ [\hat{i}_{mr}]\ = -\hat{i}_{mr}\ +\ i_{ed} \tag{32}$$

$$\omega_m = \frac{i_{eq}}{\tau_r\ \hat{i}_{mr}}\ +\ \omega_r \tag{33}$$

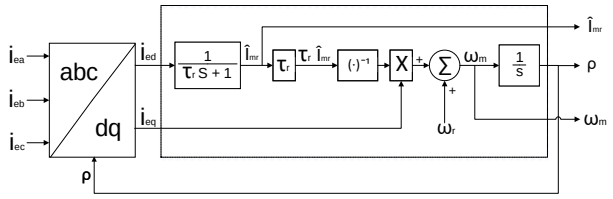

Fig. 5. Flux observer block diagram.

C. Vector control of SCIG in rotor field coordinates

The vector control of the SCIG as a function of the coordinates of the rotor field is shown in the block diagram of Fig. 6. This control is implemented from (32) and (28) to obtain i_{edref} and i_{eqref} of the generator.

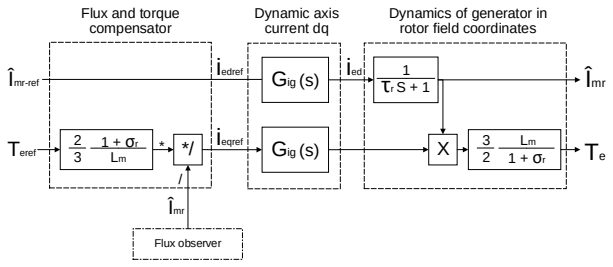

Fig. 6. Block diagram of the vector control of the SCIG as a function of the coordinates of the rotor field.

The reference magnetizing current and the reference electric torque are obtained by (34) and (35), in which V_{en} is the nominal line rms voltage of the stator and ω_{m0} is the nominal angular velocity of the generator ($\omega_{m0}\ =\ 2\ \pi\ f_{m0}$) and P_{ref} is the desired reference power.

$$\hat{i}_{mr-ref} = \sqrt{\frac{2}{3}}\ \frac{V_{en}}{(1\ +\ \sigma_e)\ L_m\ \omega_{m0}} \tag{34}$$

$$T_{eref} = \frac{P_{ref}}{\omega_r} \tag{35}$$

D. IGSC current control

The block diagram representation of the dq axis current controllers of the IGSC is presented in Fig. 7, while Fig. 8 shows the simplified diagram.

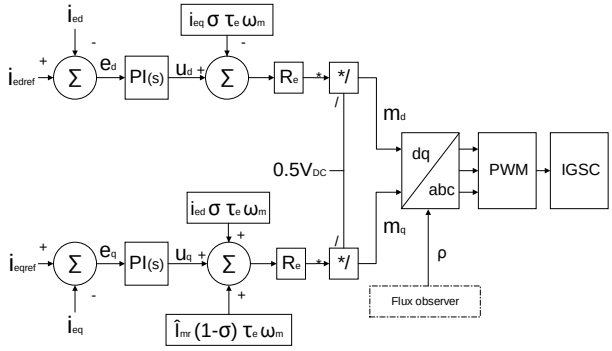

Fig. 7. IGSC Current Control System.

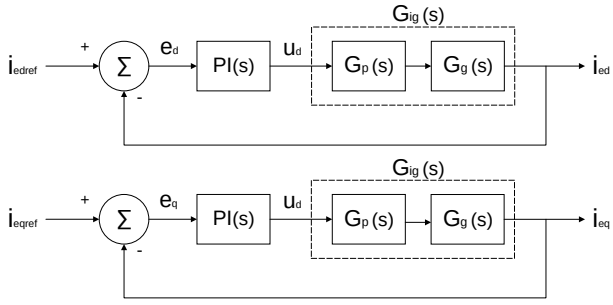

Fig. 8. Simplified block diagrams of IGSC electrical current controllers at dq coordinates.

The block $PI(s)$ is a PI controller, $G_p(s)$ represents the PWM dynamics of the DC-AC electronic converter, and $G_g(s)$ is the IGSC plant. $G_{ig}(s)$ is the product of blocks $G_p(s)$ and $G_g(s)$ in cascade. $G_g(s)$ is defined in (36).

$$G_g(s) = \frac{1}{\sigma\tau_e s\ +\ 1} \tag{36}$$

Applying the design methodology of the PI controllers and adopting $\omega_c\ =\ 500\ rad/s$ and $PM\ =\ 60^{\text{o}}$, it was obtained $k_p = 6.3986$ and $T_i = 0.0028$ for the IGSC current controllers.

IV. Results

The wind power generation system shown in Fig. 1 was implemented in software $Matlab/Simulink^{©}$. The generation system parameters used in the simulation are shown in Table I, so that the IGSC parameters were obtained in [5]. The switching frequency of the converters is 10 kHz.

The simulation of the wind generation system was carried out with variable speed, in which the generator operates with a speed of 150 rad/s and 200 rad/s, according to Fig. 9.

TABLE I
Simulation Parameters

	Parameters	Values
SCIG	P_n, V_n, F_n, P	$15kW$, $460V$, $60Hz$, 4
SCIG	R_e, R_r, L_e = L_r	$276.1m\Omega$, $164.5m\Omega$, $78.3mH$
SCIG	L_m, L_{le}, L_{lr},	$76.14mH$, $2.191mH$, $2.191mH$
Converter	C_{DC}, V_{DC}	$3500\mu F$, $800V$
Grid	V_{LL}, F, R_g, L_g	$380V$, $60Hz$, $0,8\Omega$, $6mH$

The GSC control consists of the components: DC bus voltage control and current control.

The Figures 10, 11 and 12 show the results obtained for DC bus voltage control and current control.

The Fig. 10 shows the reference voltage of the DC bus and the measured voltage on the DC bus. It was verified that the DC bus voltage control remains stable and regulated at 800 V even with the speed variation of the electric generator.

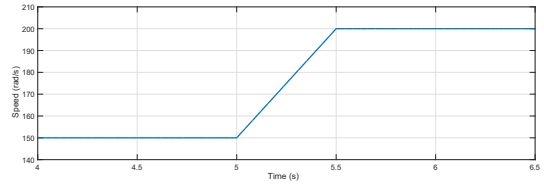

Fig. 9. SCIG rotor speed ramp from 150 rad/s to 200 rad/s.

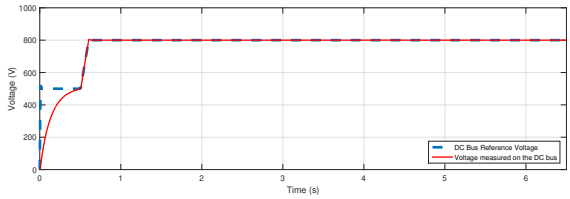

Fig. 10. Reference voltage of the DC bus and measured voltage of the DC bus.

The Figures 11 and 12 show the responses of the GSC currents control, i_d and i_q, following their references, i_{dref} and i_{qref}, showing the good functioning of the control.

In Fig. 10, it observes i_d presents negative values from 0.5s to 0.6s, since in this time interval the DC bus voltage reaches 800V, and current from the grid to the converter that requires power. After the DC bus voltage stabilizes at 0.6s, i_d remains constant at zero up to 4.0s. From 4.0s, i_d presents an increasing

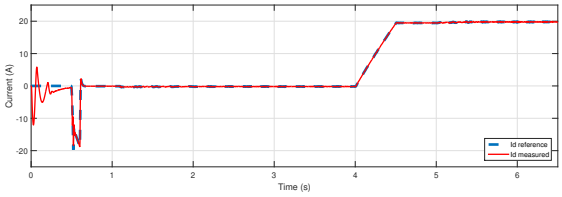

Fig. 11. Reference direct axis current and measured direct axis current.

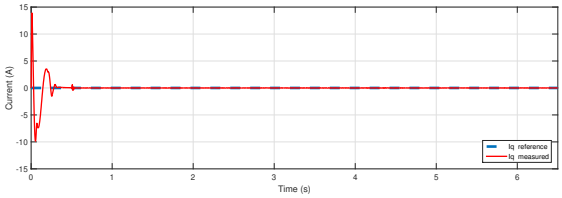

Fig. 12. Reference quadrature axis current and measured quadrature axis current.

positive value when the generator starts supplying active power to the grid because i_d is directly proportionally to the active power delivered to the grid. The current i_q is maintained at 0A, keeping the reactive power sent to the grid at zero, being the reactive power controlled by i_q.

Figures 13 and 14 illustrate the measured magnetizing current of the generator and its reference, and measured torque of the generator and its reference. As can be seen, the magnetization current and the torque follow its references, which proves the suitable functioning of the control. It is also observed that the torque changes according to the variation of the generator speed.

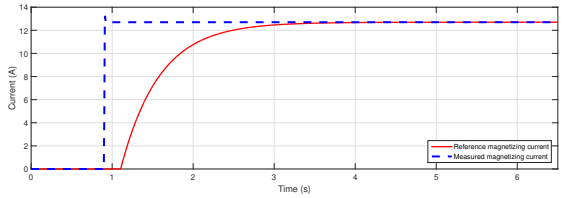

Fig. 13. Reference magnetizing current and magnetising current measured from generator.

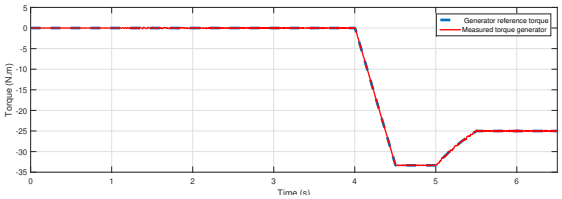

Fig. 14. Torque reference and measured torque of the generator.

Figures 15 and 16 show the responses of IGSC current control loops, i_{ed} and i_{eq}, following their references, i_{edref} and i_{eqref}.

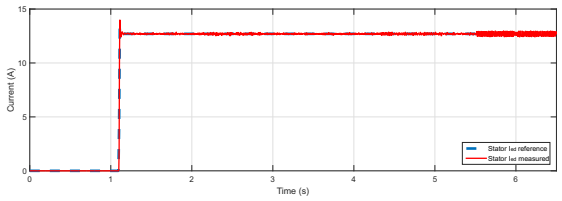

Fig. 15. Direct stator reference axis current and stator direct axis current measured.

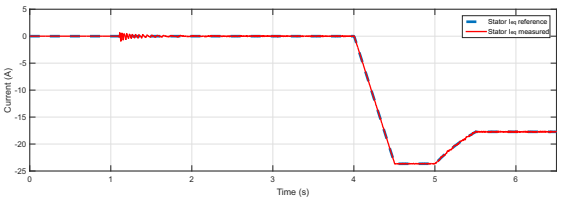

Fig. 16. Stator reference quadrature axis current and stator measured quadrature axis current.

It is verified that i_{eq} is controlled by torque. When torque varies i_{eq} changes. It is also observed that i_{ed} follows its reference from the IGSC current control.

The Figures 17, 18 and 19 illustrate a comparative of the system powers during the speed variation of the generator shown in Fig. 9, where P1 is the power delivered by the generator to the IGSC, P2 is the power received by the GSC, and P3 is the power delivered to the power grid.

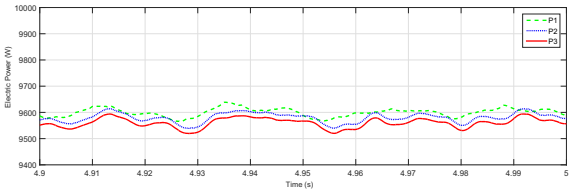

Fig. 17. Comparison of powers measured throughout the system between 4.90s and 5.0s.

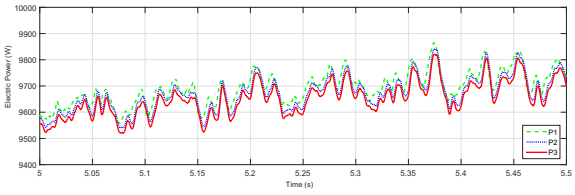

Fig. 18. Comparison of powers measured throughout the system between 5.0s and 5.5s.

From Figures 17, 18 and 19 it is possible to observe the difference of the power values during the operation of the system. The power values are decreasing during the course of the system, which is due to the switching losses of the converters.

In addition, it is noted that the powers increase with increasing speed, and the Figures 17, 18 and 19 show that the higher the speed of operation of the generator, the higher the power delivered to the grid.

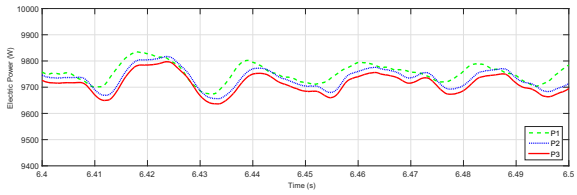

Fig. 19. Comparison of powers measured throughout the system between 6.40s and 6.50s.

V. Conclusions

This research investigated the behavior of a wind power system with SCIG. The controllers of the wind power system were calculated by the presented methodology and it was verified a suitable behavior of the control, which was observed with the results obtained from the DC bus voltage control, GSC current control and IGSC current control. From the results it was also observed the active power delivered to the grid, noting that the increase of the generator speed caused the increase of the power generated and delivered to the grid.

Acknowledgment

This work was supported by FUNCAP grant code BP3-0139-00022.01.00/18.

References

[1] Adson Bezerra Moreira, Tárcio A. S. Barros, Vanessa S. C. Teixeira, Paulo S. Nascimento Filho, and Ernesto Ruppert Filho, "Controle de Potências para Geração Eólica e Filtragem de Corrente Harmônica com Gerador de Indução Duplamente Alimentado," An. do VI Simpósio Bras. Sist. Elétricos, 2016.

[2] T. A. Lipo, "Vector control and dynamics of AC drives," [S.l.]: Oxford university press, 1996.

[3] A. Yazdani and R. Iravani, "Voltage-sourced converters in power systems: modeling, control, and applications," [S.l.]: John Wiley Sons, 2010.

[4] K. Ogata, "Engenharia de Controle Moderno," 5ªed., [S.l.]: Pearson, 2011.

[5] M. HEYDARI, A. Y. VARJANI and M. MOHAMADIAN, "A Novel Variable-Speed Wind Energy System Using Induction Generator and Six-Switch AC/AC Converter," 2012 3rd Power Electronics and Drive Systems Technology (PEDSTC), 2012.

[6] W. Suebkinorn and B. Neammanee, "An implementation of field oriented controlled SCIG for variable speed wind turbine," Proc. 2011 6th IEEE Conf. Ind. Electron. Appl. ICIEA 2011, pp. 39–44, 2011.

[7] S. Mahajan, S. K. Subramaniam, K. Natarajan, A. G. Nanjappa Gounder, and D. V. Borru, "Analysis and control of induction generator supplying stand-alone AC loads employing a Matrix Converter," Eng. Sci. Technol. an Int. J., vol. 20, no. 2, pp. 649–661, 2017.

[8] H. Merabet Boulouiha, A. Allali, M. Laouer, A. Tahri, M. Denaï, and A. Draou, "Direct torque control of multilevel SVPWM inverter in variable speed SCIG-based wind energy conversion system," Renew. Energy, vol. 80, pp. 140–152, 2015.

[9] Y. Chen, Y. Yang, L. Wang, Z. Jia, and W. Wu, "Grid-connected and control of MPPT for wind power generation systems based on the SCIG," CAR 2010 - 2010 2nd Int. Asia Conf. Informatics Control. Autom. Robot., vol. 3, no. 5, pp. 51–54, 2010.

[10] M. Benchagra, M. Maaroufi, and M. Ouassaid, "Study and analysis on the control of SCIG and its responses to grid voltage unbalance," Int. Conf. Multimed. Comput. Syst. -Proceedings, no. 4, pp. 1–5, 2011.

[11] M. A. H. Navas, J. L. A. Puma, and A. J. S. Filho, "Direct torque control for squirrel cage induction generator based on wind energy conversion system with battery energy storage system," 2015 IEEE Work. Power Electron. Power Qual. Appl. PEPQA 2015 - Proc., no. July 2018, 2015.